International Journal of Modern Studies in Mechanical Engineering (IJMSME)
Volume 4, Issue 4, 2018, PP 16-29
ISSN 2454-9711 (Online)
DOI: http://dx.doi.org/10.20431/2454-9711.0404003
www.arcjournals.org

Influence of Rotation on the Heat and Fluid Flow around a Circular Cylinder

Rahim Hassanzadeh*, Mohsen Darvishyadegari

Department of Mechanical Engineering, Urmia University of Technology, Urmia, Iran

Corresponding Author:** ***Rahim Hassanzadeh*, Department of Mechanical Engineering, Urmia University of Technology, Urmia, Iran*

Abstract: *Heat and fluid flow around a rotating cylinder in the free-stream flow at the Reynolds number of 200 is numerically investigated by means of the finite volume approach. Computations are performed using different counter-clockwise non-dimensional rotating speeds (RS) between the 0 and 4. The obtained results are validated against the available data. It is found that proportional to the RS, an asymmetric flow topology is developed around the cylinder which causes to an increase on the lift coefficient and a decrease on the drag coefficient. In addition, instabilities of the shear layer are reduced proportion to RS due to suppression the wake and dominating the rotating flow around the cylinder. On the other hand, it is revealed that rotating the cylinder decreases the rate of heat transfer between the hot cylinder and surrounding fluid flow, generally. Finally, it is demonstrated that both vortex shedding process and rotation of the cylinder have influences on the heat transfer process.*

Keywords: *Convective Heat Transfer, Rotating Cylinder, Vortex Shedding, Shear Layer, Fluid Rotating Zone*

1. INTRODUCTION

Heat transfer and fluid flow around a stationary circular cylinder have been a subject of numerous previous studies not only using the different computational methods but also by means of various experiments [1-6]. This is due to fundamental flow physics regarding a circular cylinder. On the other hand, heat and fluid flow around a circular cylinder is the subject of significant numbers of industrial applications such as heat exchangers, offshore structures, heating and cooling systems, transmission cables, high-rise buildings, and bridge piers.

Flow nature around a circular cylinder is strongly depended to the Reynolds number. That is, at low Reynolds numbers, the separated flow downstream of the cylinder is stable. By increasing the Reynolds number to the critical limit, instabilities occur in shear layer and vortex shedding process dominants. The shed vortices frequency is also depended to the Reynolds number. At the Reynolds number of 200, although the vortex shedding process exists, however, the flow nature is laminar.

Rotating the cylinder in the free-stream flow is a process in which the vortex shedding mechanism affects, significantly. In this process, heat and momentum transfer change with RS. There are some restricted studies on the flow around a rotating cylinder. Most of the previous numerical and experimental are focused on the vortex shedding process downstream of a rotating cylinder. Rao et al. [7] conducted on flow over a rotating cylinder located on a flat wall and focused on the wake structure downstream of the rotating cylinder. Effects of the RS and gap space between the rotating cylinder and wall have been discussed in their study. In a similar work, Rao et al. [8] revealed that proportional to the gap space, the value of the drag coefficient for a rotating cylinder increases. In another work, Dipankar and Sengupta [9] investigated the flow past a circular cylinder in the vicinity of a plane wall. They showed that the gap space between the circular cylinder and wall plays an important role in the cylinder-wall interaction. Abrahamsen Prsic et al. [10] used Large Eddy Simulation to study the flow around a circular cylinder close to a flat seabed at Re=13100. They indicated that for smaller gap space than the critical value, the vortex shedding is suppressed and by increasing the gap space, an asymmetric vortex shedding process can be developed. In addition, at large gap spaces, a periodic separation occurs from the sides of the cylinder. Afroz et al. [11] studied the adverse pressure gradient generation over a flat plate using a rotating cylinder. They applied two different Reynolds number of

200 and 1000 and obtained several results. For example, they indicated that the vortex shedding strongly depends on the gap size and RS. At any specific gap height, the vortex shedding is suppressed above a threshold value of cylinder rotating speed producing a steady wake. Thakur et al. [12] presented a research work on the motion of a rotating circular cylinder in a stream of Bingham plastic fluid at small Reynolds number in the range of $0.1 \leq Re \leq 40$. It was shown that the rotation enhances the stability of the flow by suppressing the flow separation. Large Eddy Simulation of a high-Reynolds number flow past a rotating cylinder was conducted by Karabelas [13]. The Reynolds number was 140000 and simulations were carried out at different RS values between 0 and 2. It was demonstrated that by increasing the RS, lift coefficient increases while the drag coefficient decreases. Lam [14] studied the vortex shedding process downstream of the rotating cylinder at $3600 \leq Re \leq 5000$. It was revealed that the vortex shedding process can be evidenced only for RS values less than 1.9.Ghazanfarian and Nobari [15] presented a numerical study on the convective heat transfer from a rotating cylinder with cross-flow oscillation at the Reynolds numbers of 50, 100, and 200 and Prandtl numbers of 0.7, 6, and 20. It was found that similar to the fixed cylinder, beyond a critical RS, vortex shedding is mainly suppressed. In addition, by increasing the RS, both the Nusselt number and the drag coefficient decrease, rapidly. Ikhtiar et al. [16] conducted on the free-stream flow and forced convection heat transfer around a rotating circular cylinder subjected to a single gust impulse for the Reynolds number in the range of $80 \leq Re \leq 160$. They found that the upstream gust causes the average Nusselt number to increase in the first and the second vortex shedding regimes but interestingly, the pattern is reversed in the intermediate vortex suppression region. Effects of Prandtl number and rotation on the vortex shedding behind a circular cylinder subjected to cross buoyancy at subcritical Reynolds number of 40 are the subject of a research presented by Chatterjee and Sinha [17]. They used three different types of fluids having Prandtl numbers of Pr=0.71, 7, and 100. It was found that the heat transfer rate decreases with RS at the critical Richardson number and it increases with increase in the Prandtl number. Heat and fluid flow across a rotating cylinder dissipating uniform heat flux in 2D laminar flow regime was presented by Paramane and Sharma [18]. In their study, the value of the Reynolds number varies from 20 to 160. It was demonstrated that average Nusselt number was found to decrease with increasing the RS and increase with increasing the Reynolds number. Recently, Hassanzadeh [19] investigated on the effects of unsteady flow generated by a rotating cylinder on the cooling mechanism of a hot plate. The value of the Reynolds and Prandtl numbers was 200 and 7.0, respectively and computations were carried out at different RS and G/D values. It was concluded that the maximum heat transfer rate between the generated unsteady flow and the hot plate occurs at G/D=0.5 at each individual RS value. Convective heat transfer and fluid flow of two counter-rotating cylinders in the tandem arrangement was the subject of a research work presented by Darvishyadegari and Hassanzadeh [20]. They performed their research at Re=200 and RS in the range between the 0 and 4. Several results have been reported in their works. For example, for both upstream and downstream cylinders, it was shown that with rotation the cylinders, the negative pressures show a tendency to become dominant all over the surface, and with increasing the RS, this negative pressure enhances considerably. In addition, at low RS values, the half-upper side of the upstream cylinder dissipates a higher amount of the heat into the surrounding fluid in comparison with the half-lower side, and vice versa for the downstream cylinder. However, at the higher RS values, due to dominating the fluid-rotating zone around both upstream and downstream cylinders, it seems that all points on each cylinder have identical roles in the heat transfer process.

A general review of the similar published works shows that the heat transfer and fluid flow characteristics are not presented in detail at least for laminar shedding process over a rotating cylinder in the free-stream. Therefore, this study is an attempt in this direction which tries to reveal more information about the hydrodynamic and thermal interactions between the rotating cylinder and the free-stream flow at Re=200.

2. NUMERICAL SETUP AND COMPUTATIONAL PROCEDURE

In the present study, in order to model the problem, a two-dimensional flow domain as shown in figure 1 is defined. The constructed flow domain has dimensions of 31D and 21D in stream wise and vertical directions, respectively. The center of rotating cylinder is exerted at x=10.5D and y=0. The origin of coordinates is set at the center of inlet section. The cylinder rotates in the counterclockwise direction with various RS values in the range of 0 and 4. An advanced multi-block grid system is constructed for the physical media. For this purpose, the flow domain is divided to several blocks and

after that, an advanced grid is constructed for each block in which the grids have minimum element size on the cylinder surface and by getting away from the cylinder surface the size of elements increases gradually using a specific ratio.

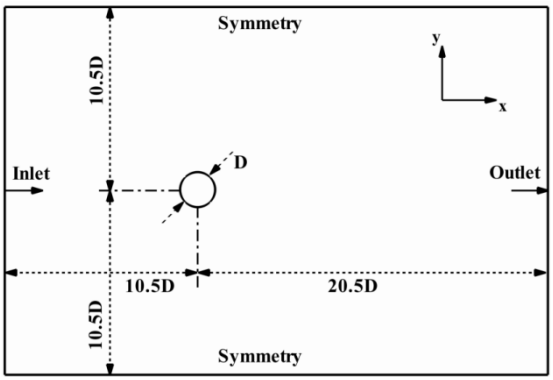

Figure1. *The applied physical flow domain*

Nomenclature

Parameter	Description
A	Area
C_D	Drag coefficient ($=\frac{F_D}{0.5\rho U^2 A}$)
C_L	Lift coefficient ($=\frac{F_L}{0.5\rho U^2 A}$)
C_p	Pressure coefficient ($=\frac{p-p_\infty}{0.5\rho U^2}$)
c_p	Specific heat
D	Cylinder diameter
F_1	Upper vortex (upper focus)
F_2	Lower vortex (lower focus)
F_D	Drag force
F_L	Lift Force
k	Conductivity
Nu	Local Nusselt number
$\overline{Nu}$	Mean Nusselt number
p_∞	Free-stream pressure
p	Pressure
Pr	Prandtl number ($=\frac{\mu c_p}{k}$)
r	Radial coordinate
r^*	Non-dimensional radius
Re	Reynolds number ($=\frac{\rho UD}{\mu}$)
RS	Non-dimensional rotating speed ($=\frac{U_T}{U}$)
SP	Stagnation point
t	time
T	Temperature
u	Streamwise velocity
u_{rms}	Root mean square of the streamwise velocity
U	Free-stream velocity
U_T	Tangential velocity
u^*	Non-dimensional streamwise velocity ($=\frac{u}{U}$)
v	Vertical velocity
v_{rms}	Root mean square of the vertical velocity

v^*	Non-dimensional vertical velocity ($=\frac{v}{U}$)
x	Streamwise dimension of coordinates
X	Non-dimensional streamwise dimension of coordinates ($=\frac{x}{D}$)
y	Vertical dimension of coordinates
Y	Non-dimensional vertical dimension of coordinates ($=\frac{y}{D}$)
Greek symbols	
μ	Dynamic viscosity of the fluid
ρ	Density of the fluid
τ	Non-dimensional time ($=\frac{tU}{D}$)
α	Angular location
θ^*	Non-dimensional temperature ($=\frac{T-T_\infty}{T_s-T_\infty}$)
Subscripts	
s	Surface of the cylinder
∞	Free-stream

The governing equations for the Newtonian, incompressible, and unsteady heat and fluid flow in two dimensions are as,

$$\frac{\partial u^*}{\partial X}+\frac{\partial v^*}{\partial Y}=0 \tag{1}$$

$$\frac{\partial u^*}{\partial \tau}+u^*\frac{\partial u^*}{\partial X}+v^*\frac{\partial u^*}{\partial Y}=-\frac{\partial p^*}{\partial X}+\frac{1}{\mathrm{Re}}\left(\frac{\partial u^*}{\partial X}+\frac{\partial u^*}{\partial Y}\right) \tag{2}$$

$$\frac{\partial v^*}{\partial \tau}+u^*\frac{\partial v^*}{\partial X}+v^*\frac{\partial v^*}{\partial Y}=-\frac{\partial p^*}{\partial Y}+\frac{1}{\mathrm{Re}}\left(\frac{\partial v^*}{\partial X}+\frac{\partial v^*}{\partial Y}\right) \tag{3}$$

$$\frac{\partial \theta^*}{\partial \tau}+u^*\frac{\partial \theta^*}{\partial X}+v^*\frac{\partial \theta^*}{\partial Y}=\frac{1}{\mathrm{Re}\,\mathrm{Pr}}\left(\frac{\partial \theta^*}{\partial X}+\frac{\partial \theta^*}{\partial Y}\right) \tag{4}$$

The momentum and energy equations are discretized using the second-order upwind scheme and for coupling of the velocity and pressure fields, the Semi-Implicit Method for Pressure-Linked Equation (SIMPLE) [21] is applied. The following boundary conditions are imposed inthe physical flow domain:

At inlet section,

$$u^*=1,\quad v^*=0,\quad \theta^*=0 \tag{5}$$

At outlet section,

$$\frac{\partial u^*}{\partial X}=0,\quad \frac{\partial v^*}{\partial X}=0,\quad \frac{\partial \theta^*}{\partial X}=0 \tag{6}$$

At side walls,

$$\frac{\partial u^*}{\partial Y}=0,\quad \frac{\partial v^*}{\partial Y}=0,\quad \frac{\partial \theta^*}{\partial Y}=0 \tag{7}$$

On the rotating cylinder,

$$u^*=-(RS)\sin\theta,\quad v^*=(RS)\cos\theta,\quad \theta^*=1 \tag{8}$$

The discretized equations are solved implicitly using the aforementioned boundary conditions by means of the finite volume method. In addition, the convergence of 3D velocity components is established at each time step by controlling the residuals of all equations which are defined to be solved by setting their variations less than 10^{-8}. The value of the Reynolds number is 200 based on the cylinder diameter and free-stream velocity and computations are carried out for a constant Prandtl number of 7.0. Furthermore, several non-dimensional rotating speeds ($RS=U_T/U$) in the range of $0 \leq RS \leq 4$ are considered for the cylinder in the counterclockwise direction. The dimensionless parameters are computed using the following equations;

- Drag coefficient

$$C_D = \frac{F_D}{0.5\rho U^2 A} \tag{9}$$

- Lift coefficient

$$C_L = \frac{F_L}{0.5\rho U^2 A} \tag{10}$$

- Pressure coefficient

$$C_p = \frac{p - p_\infty}{0.5\rho U^2} \tag{11}$$

- Local Nusselt number

$$Nu = -\frac{\partial \theta^*}{\partial r^*}\bigg|_{r^*=0} \tag{12}$$

In which,

$$r^* = \frac{r}{D} \tag{13}$$

- Time-averaged Nusselt number

$$\overline{Nu} = \frac{1}{\Delta t}\int_t^{t+\Delta t} Nu dt \tag{14}$$

3. Grid Size Independence Study

In order to find an optimum grid number with sufficient resolution, five different grid resolutions are examined in this study. Table 1 shows details of the examined grid systems. Computations are demonstrated ignorable sensitivity to applied grid resolutions as illustrated in Table 2 which compares the values of time-averaged lift and drag coefficients as well as the Nusselt number under five different grid resolutions at RS=0. Therefore, the fourth grid system is applied for all simulations with24550 control volumes.

Table1. *Details of grid size independence study*

Grid	Control volume No.	Faces No.	Node No.
1	6452	13091	6639
2	10002	20237	10235
3	15712	31716	16004
4	24550	49465	24915
5	39012	78484	39472

Table2. *Results of grid size independence study*

Grid	C_L, max	Error (%)	C_D	Error (%)	$\overline{Nu}$	Error (%)
1	±0.787	-----	1.386	-----	17.92	-----
2	±0.764	2.92	1.387	0.072	17.75	-0.948
3	±0.744	2.61	1.383	-0.288	17.69	-0.338
4	±0.727	2.28	1.381	-0.144	17.66	-0.169
5	±0.716	1.51	1.376	-0.362	17.63	-0.169

4. Validation Of Numerical Results

In order to validate the applied numerical code in this study, some key parameters such as the time-averaged drag coefficient and maximum lift coefficient are compared with previous studies in table 3. In addition, the obtained time-averaged Nusselt number for the stationary cylinder is compared with available correlations as well as the previous data in table 4. The comparisons show good agreements between the results of the present study with that of the other researches as shown in tables 3 and 4.

Table3. *Validation of the Lift and Drag results at Re=200*

Author	$C_{L,\,max}$	C_D
Rajani et al. [2]	---	1.33
Al-Mdallal [22]	±0.69	1.31
Henderson [23]	---	1.34
Meneghini and Bearman [24]	±0.59	1.23
Wen and Lin [25]	---	1.30

Poncet [26]	±0.70	1.34
Mahir and Altac [27]	±0.69	1.376 ± 0.048
Liu et al. [28]	±0.69	1.31 ± 0.049
Ding et al. [29]	±0.65	1.348 ± 0.050
Braza et al. [30]	±0.75	1.40 ± 0.05
Present study	±0.71	1.376

Table4. *Comparison of the obtained time-averaged Nusselt number in the present study for stationary cylinder with available correlations and data at Re=200 and Pr=7.0*

Correlation and data	$\overline{Nu}$
Hilpert and Forsch [31]	15.43
Churchill and Bernstein [32]	16.63
Harimi and Saghafian [33]	16.39
Present study	17.65

5. Results And Discussions

Figure 2 presents time-averaged streamlines around the rotating cylinder under different non-dimensional rotating speeds such as RS=0, 1, 2, 3, and 4. The RS=0 is corresponded to the stationary cylinder and well documented in the literature. For the stationary cylinder, the interaction between the circular cylinder and the free-stream flow develops a wake downstream of the cylinder. In the wake, a well-defined recirculating region is seen very close to the cylinder. Development of a recirculating region is due to flow separation from the sides of the cylinder. Inside the recirculating region, upper focus, F_1, and lower focus, F_2, and saddle point, S, are clearly seen in figure 2. Here, the saddle point, S, is defined as a point in which the upper focus, F_1, and lower focus, F_2, merge to each other. By rotating the cylinder in the counterclockwise direction, this symmetric structure is deflected in which the rate of this deflection is proportional to the RS. In the case of RS=1, as a low rotating speed, the size of lower focus, F_2, becomes minimum while the upper focus, F_1, shrinks due to rotational effects. Therefore, the locations of the saddle point and stagnation point, SP, move toward the upper side as illustrated in figure 2. At higher rotating speed such as RS=2, the lower focus is eliminated and more displacement of the saddle point and stagnation point toward the upper side is evidenced as indicated in the case of RS=2. Beyond the RS=2, rotating flow around the cylinder becomes strong and consequently, the recirculating region disappears for RS=3 and 4. An interesting result can be seen in the case of RS=4 in which the flow topology seems to become symmetry with respect to the vertical axis passing from the center of the cylinder. As a result, rotating the cylinder suppresses the shear layer and hence, proportional to the RS, reduction in the shear layer instabilities is expected. The obtained results are in good agreement with data reported by previous researchers [11, 13, 14].

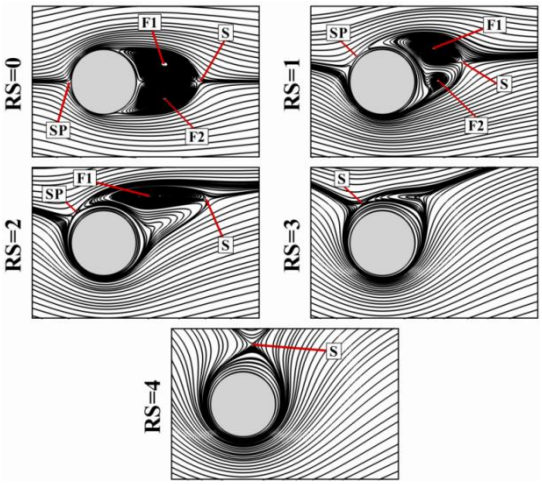

Figure2. *Time-averaged streamlines around a rotating cylinder under different rotating speeds of RS=0, 1, 2, 3, and 4*

Variations of time-averaged streamwise velocity on a defined horizontal line downstream of the cylinder are illustrated in figure 3 for RS=0, 1, 2, 3, and 4. Here, the values of the streamwise velocity and distance are normalized using the free-stream velocity and the cylinder diameter, respectively. In the case of RS=0, streamwise velocity has negative values just downstream of the cylinder. This is

due to the development of the recirculating region around the cylinder. After that, velocity magnitude takes positive values and gradually enhances in the streamwise direction. Rotating the cylinder causes a sudden increase in the streamwise velocity because of the gradual shrinking and elimination of the recirculating region downstream of the cylinder. On the other hand, dominating the main flow in the core region downstream of the cylinder is occurred earlier for rotating cases in comparison to the stationary case.

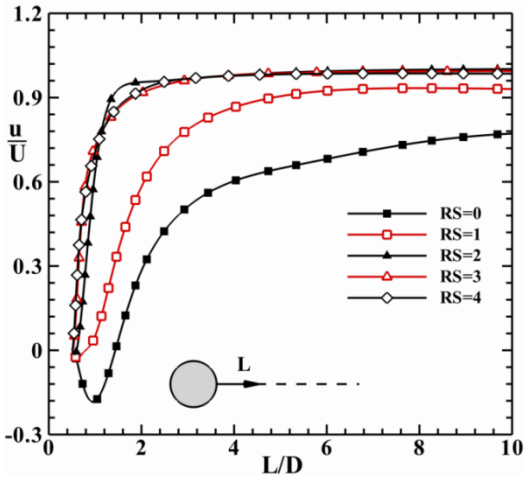

Figure3. *Distribution of time-averaged non-dimensional streamwise velocity downstream of the rotating cylinder under different rotating speeds of RS=0, 1, 2, 3, and 4 ("L" is measured from the rear surface of the cylinder toward the positive streamwise direction)*

Figures 4 demonstrates distributions of time-averaged non-dimensional streamwise velocity on the six vertical lines such as L/D=1, 3, 5, 7, 9, and 15 downstream of the cylinder. It should be said that "L" is measured from the center of the cylinder toward the downstream of the cylinder. Distributions of the streamwise velocity show symmetric trends on each vertical location for RS=0. In the location of L/D=1, streamwise velocity magnitudes have negative minimum value due to passing from the recirculating region. Moving far from the stationary cylinder, the minimum peak value of the streamwise velocity attenuates and becomes positive proportional to L/D value. Rotating the cylinder causes to develop an asymmetric velocity distribution downstream of the cylinder along each vertical lines. In the cases of the RS=1 and 2 at L/D=1, although the flow experiences minimum negative values, however, the minimum peak values are shifted toward the upper side of the rotating cylinder due to deflection of the wake downstream of the cylinder. Further downstream of the cylinder, effects of the rotation on the wake deflection are still observable since the core of the minimum velocity magnitudes is moved toward the upper side of the rotating cylinder at RS=1 and 2.Beyond the RS=2, it seems, more or less, a symmetric streamwise velocity distribution is dominated on the half-upper and half-lower sides of the cylinder all over the wake.

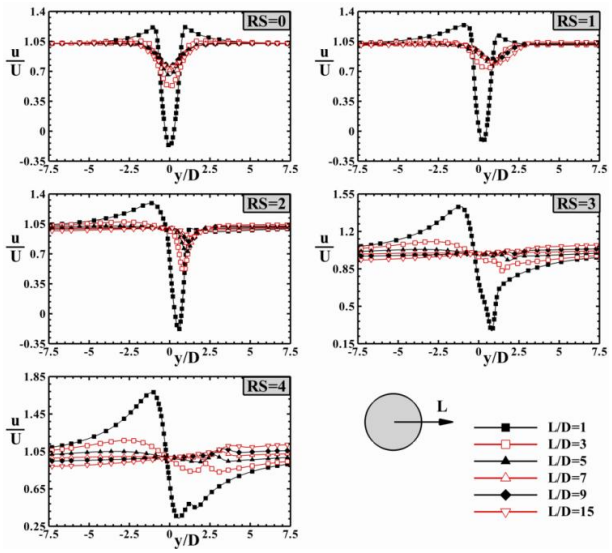

Figure4. *Distribution of time-averaged non-dimensional streamwise velocity along the several vertical lines such as L/D=1, 3, 5, 7, 9, and 15 under different rotating speeds of RS=0, 1, 2, 3, and 4 ("L" is measured from the center of the cylinder toward the positive streamwise direction)*

Figure 5 presents the distributions of time-averaged non-dimensional vertical velocity on the six vertical lines such as L/D=1, 3, 5, 7, 9, and 15 downstream of the cylinder. In the RS=0, as seen, a symmetric distribution is developed on each individual line in the absence of the rotational effects. In other words, at each upper and lower sides of the wake, a peak value is developed in which proportional to the L/D value, the magnitudes of the peak values are diminished due to dominating the free-stream flow in the core flow, gradually. In the rotating cases, this symmetric distribution is collapsed with respect to RS value and the upper peak grows while the lower peak attenuates proportional to the RS value. Beyond the RS=3, the lower peak is completely collapsed and the upper peak is developed very close to y/D=0 as seen in figure 5.

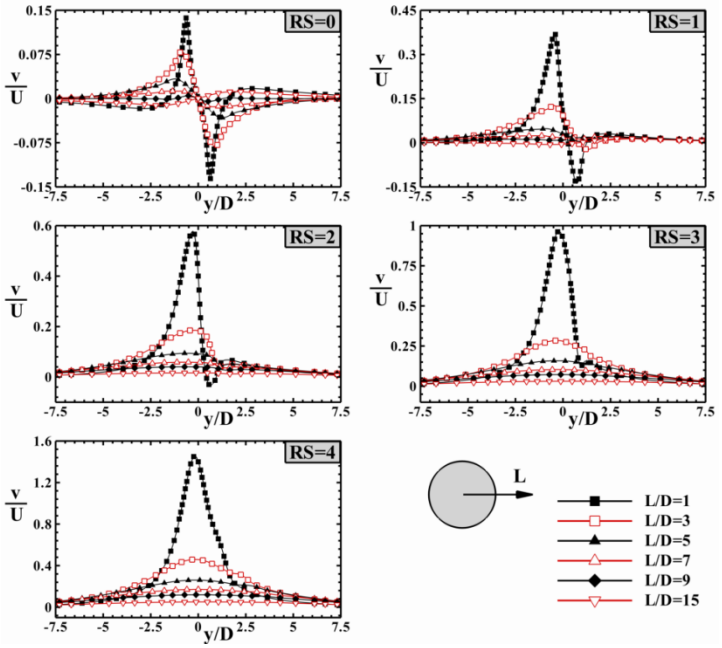

Figure5. *Distribution of time-averaged non-dimensional vertical velocity along the several vertical lines such as L/D=1, 3, 5, 7, 9, and 15 under different rotating speeds of RS=0, 1, 2, 3, and 4 ("L" is measured from the center of the cylinder toward the positive streamwise direction)*

Figures 6 and 7 show distributions of root mean square (rms) values of streamwise and vertical velocities, respectively at six different vertical locations such as L/D=1, 3, 5, 7, 9, and 15. Similar to figures 4 and 5, "L" is measured from the center of the cylinder toward the downstream of the cylinder. Both of the rms values are normalized using the free-stream velocity. As expected, in the case of RS=0, symmetric variations can be observed for all vertical locations. Maximum rates of unsteadiness for stationary cylinder in streamwise and vertical directions are obtained at L/D=3 which is out of recirculation region. It is mainly due to vortex shedding process which has significant effect in this vertical location. Beyond the L/D=3, proportional to the distance from the cylinder, the rate of unsteadiness reduces as seen for RS=0. In the case of rotating cylinder, this scenario is changed. First of all, location of maximum unsteadiness is shifted to half-upper side for each L/D. Examination of the rms values of streamwise velocity shows that the location of L/D=1 has the highest rate of unsteadiness in main flow direction for all RS values such as RS=1, 2, 3, and 4. Increasing the rate of unsteadiness in the streamwise direction at L/D=1 compared with that of L/D=3 is due to reduction in shedding mechanism and augmentation of the rotational effects. However, after the L/D=1, location of L/D=3 has the highest rate of unsteadiness in the streamwise direction for all RS values such as RS=1, 2, 3, and 4. Further downstream of the cylinder, the u_{rms}/U values change in a systematic trend proportional to the value of L/D. In the case of vertical rms values, the maximum v_{rms}/U is obtained at L/D=3 for small rotating speeds of RS=1 and 2. However, in the absence of the vortex shedding mechanism, the maximum rms values of the vertical velocity are developed at L/D=1 for RS=3 and 4. On the other hand, due to counterclockwise rotating the cylinder, the maximum v_{rms}/U values are occurred on the half-upper side of the vertical locations due to a higher rate of interaction between the free-stream flow and the rotating flow. Both u_{rms}/U and v_{rms}/U values minimize at L/D=15 as illustrated in figures 6 and 7. Furthermore, proportional to the RS, the rate of unsteadiness downstream of the cylinder reduces as indicated in figures 6 and 7.

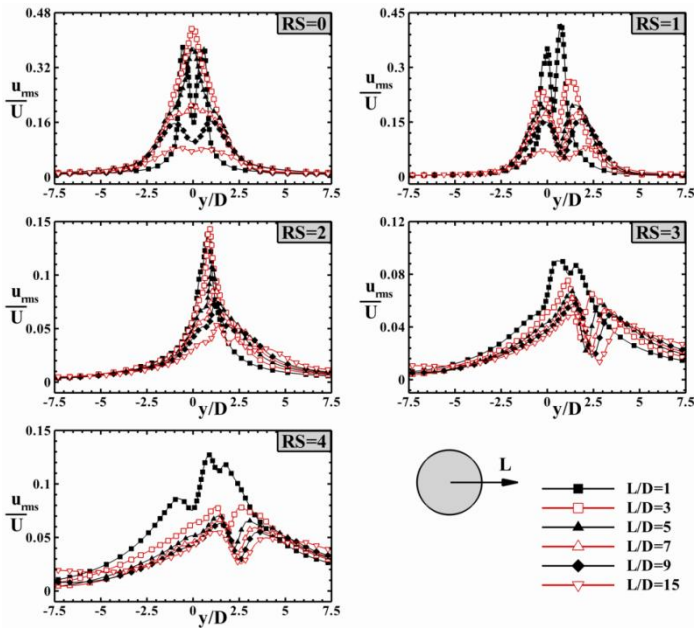

Figure6. *Distribution of the root mean square values of non-dimensional streamwise velocity along the several vertical lines such as L/D=1, 3, 5, 7, 9, and 15 under different rotating speeds of RS=0, 1, 2, 3, and 4 ("L" is measured from the center of the cylinder toward the positive streamwise direction)*

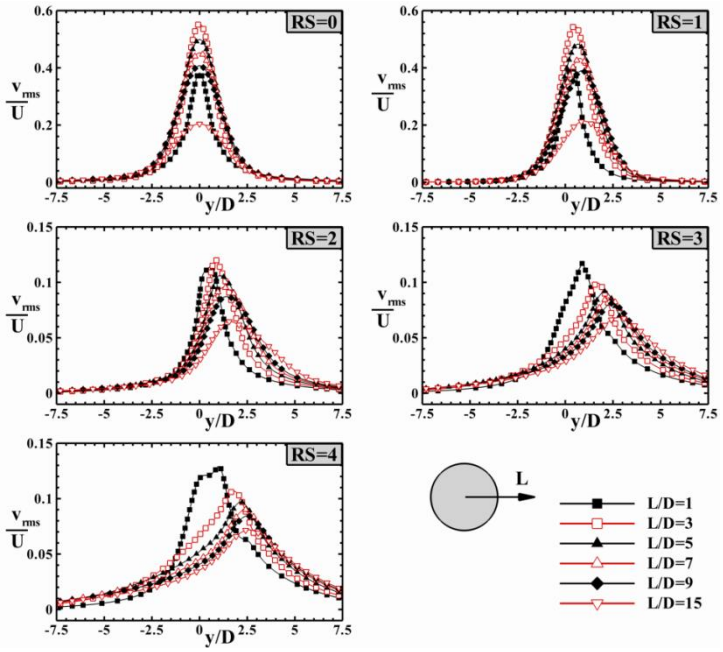

Figure7. *Distribution of the root mean square values of non-dimensional vertical velocity along the several vertical lines such as L/D=1, 3, 5, 7, 9, and 15 under different rotating speeds of RS=0, 1, 2, 3, and 4 ("L" is measured from the center of the cylinder toward the positive streamwise direction)*

Distributions of the mean pressure coefficient for rotating cylinder along the angular location are demonstrated in figure 8 for each non-dimensional rotating speed such as RS=0, 1, 2, 3, and 4. Examination of the obtained results reveals that for the stationary cylinder, the maximum positive pressure occurs at $\alpha=180^{\circ}$ which is called the front stagnation point. In agree with previous investigations [11, 13], the minimum pressure is developed at $\alpha=100^{\circ}$ on the half-upper surface and at $\alpha=260^{\circ}$ on the half-lower surface for RS=0. Rotating the cylinder develops an angular motion of the flow very close to the cylinder. Due to the counterclockwise motion of the cylinder, it is predicted that the pressure on the half-upper surface of the cylinder becomes higher in comparison to the lower surface. As seen in figure 8, rotating the cylinder leads to a displacement of the front stagnation point in the clockwise direction. That is, the location of the front stagnation point is displaced to $\alpha=160^{\circ}$, $\alpha=140^{\circ}$, and $\alpha=120^{\circ}$ for RS=1, 2, and 3, respectively. A noticeable result in this context is the development of the negative pressure all over the cylinder in the case of RS=4.In addition, the

minimum pressure is developed between $240^{\circ} \leq \alpha \leq 270^{\circ}$, for RS=1, 2, 3, and 4. Moreover, rotating the cylinder affects strongly the magnitude of the minimum pressure proportional to the RS as seen in figure 8. In brief, proportional to the RS, rotating the cylinder increases the pressure difference between the upper and lower surfaces of the rotating cylinder. It is known that development of the higher pressure difference on the cylinder surface in vertical direction absolutely increases the lift coefficient which will be discussed in this section.

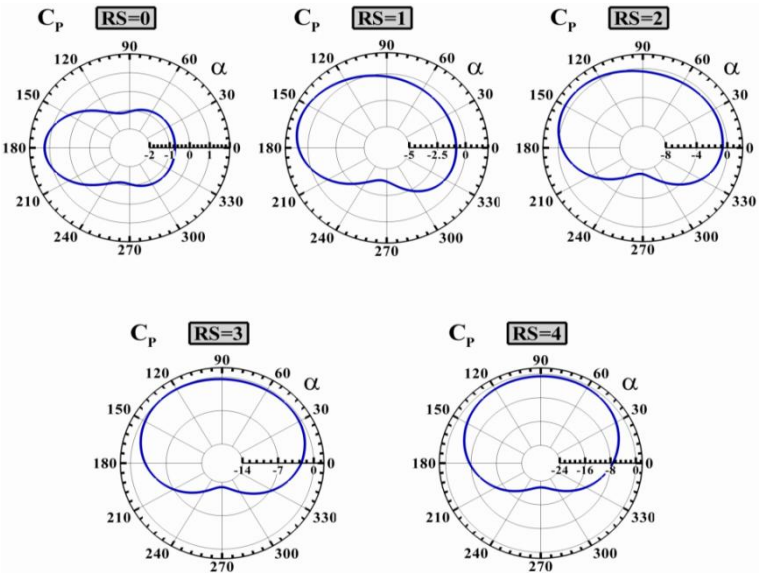

Figure8. *Distribution of time-averaged pressure coefficient along the angular location of rotating cylinder under different rotating speeds of RS=0, 1, 2, 3, and 4*

Figure 9 presents the time history of the lift and drag coefficients for different rotating speeds such as RS=0, 1, 2, 3, and 4. It is clearly seen that in the case of RS=0, lift and drag coefficients are oscillating with time. Oscillating the lift and drag coefficients are mainly due to the vortex shedding process. Rotating the cylinder with low RS attenuates the amplitude of these oscillations as seen for RS=1 since proportional to the RS, the instabilities of the shear layer reduce. These oscillations reach their minimum amplitudes in the case of RS=2. Beyond the rotating speed of "2", time histories of the lift and drag coefficients are not oscillating. As a result, proportional to the RS, instabilities of the shear layer reduces and consequently, the oscillation amplitudes of the lift and drag coefficients attenuate. In the cases of RS=3 and 4, it seems the wake downstream of the cylinder becomes stable and flow behaves like as the steady flow as illustrated in figure 9. On the other hand, due to development of an asymmetric wake over the rotating cylinder, as discussed in figure 2, the pressure difference enhances between the half-upper and half-lower sides of the rotating cylinder.

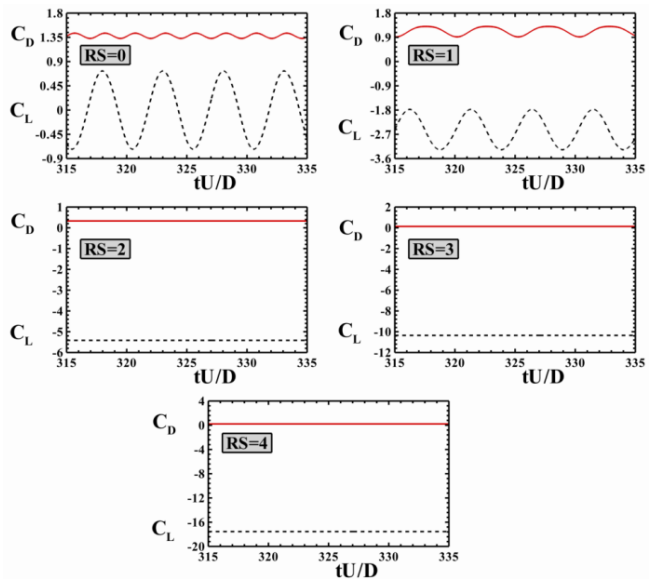

Figure9. *Time histories of lift and drag coefficients under different rotating speeds of RS=0, 1, 2, 3, and 4*

Variations of the mean drag and lift coefficients along the RS are illustrated in figure 10. According to the obtained results, increasing the RS of the cylinder reduces the drag coefficient of the cylinder due to gradual shrinking and collapsing the recirculating region downstream of the cylinder. However, since the maximum pressure location moves toward the upper side and the minimum location of the pressure is located on the lower side of the cylinder, the lift coefficient enhances, rapidly. In other words, rotating the cylinder in the counterclockwise direction leads to a tendency of the cylinder to move along the negative vertical direction.

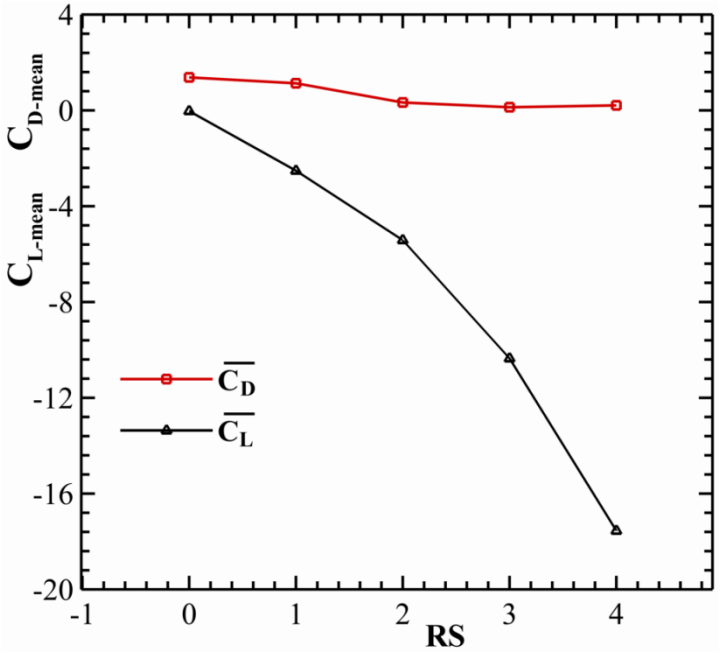

Figure10. *Variation of mean lift and drag coefficients along the rotating speed*

Figure 11 illustrates instantaneous vorticity fields for rotating speeds of RS=0 and 1. In the case of RS=0 as the stationary cylinder, vortices shed downstream of the cylinder with a periodic fashion from the upper and lower sides and moves toward the downstream of the cylinder. This periodic vortex shedding process is also seen for RS=1. Beyond the RS=1, rotating the cylinder suppresses the wake downstream of the cylinder on the upper or lower sides of the cylinder so that the periodic vortex shedding process is collapsed.

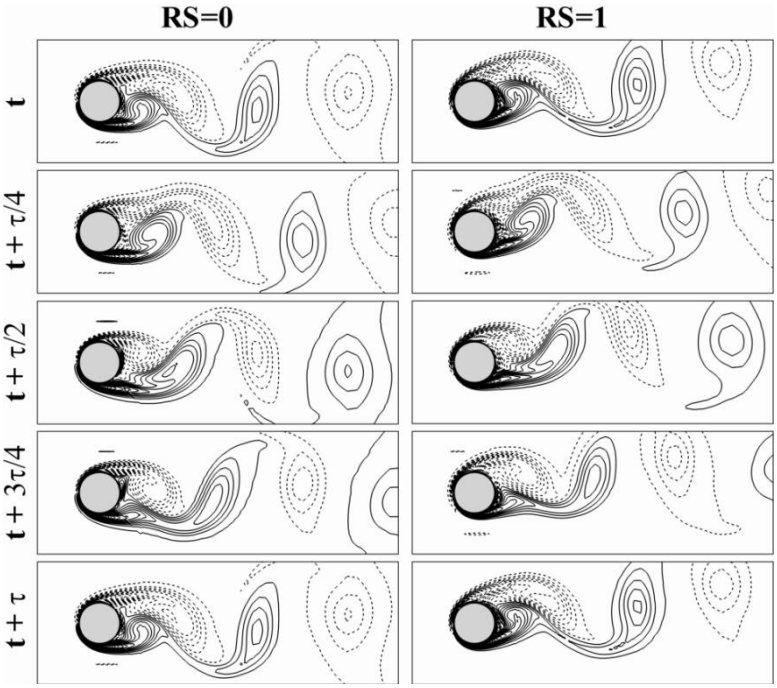

Figure11. *Instantaneous vorticity fields for RS=0 and 1*

Distribution of the time-averaged Nusselt number along the angular location is presented in figure 12 for different rotating speeds such as RS=0, 1, 2, 3, and 4.In the case of RS=0, a symmetric distribution is obtained for the Nusselt number in which the rate of heat transfer is maximum at $\alpha=180^{\circ}$(front stagnation point) and minimum at $\alpha=60^{\circ}$. The obtained trend for the Nusselt number of stationary cylinder is in good agreement with data reported by Paramane and Sharma [18]. In the case of RS=1, maximum and minimum locations of the heat transfer are located at $210^{\circ}\leq\alpha\leq240^{\circ}$ and $120^{\circ}\leq\alpha\leq150^{\circ}$, respectively. Beyond the RS=2, more or less, it can be said that a uniform local heat transfer is dominated over the cylinder due to the significant rotational effect. In other words, by increasing the RS, all locations on the cylinder show an identical contribution on the heat transfer process.

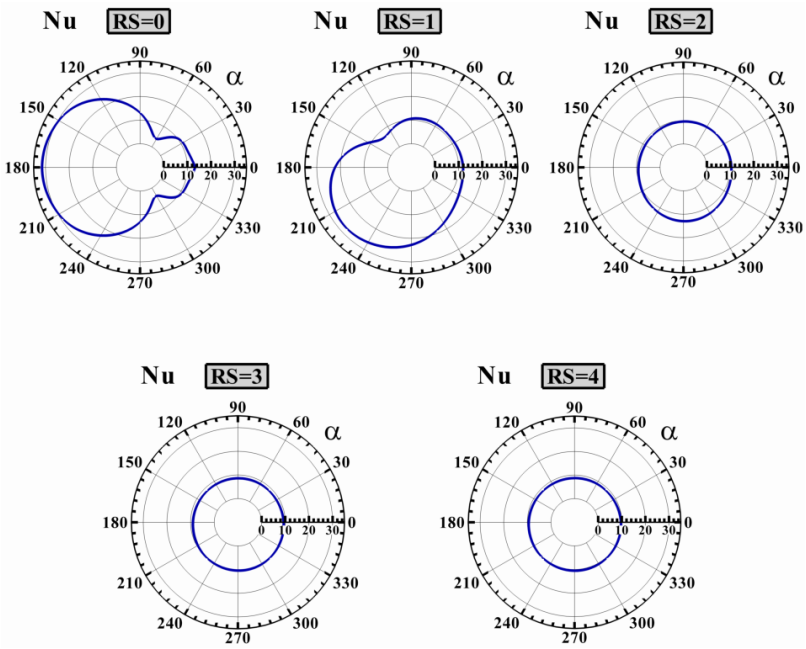

Figure12. *Distribution of time-averaged local Nusselt number along the angular location of rotating cylinder under different rotating speeds of RS=0, 1, 2, 3, and 4*

Figure 13 demonstrates the mean Nusselt number magnitudes along the RS. Clearly seen that in the case of RS=0, the magnitude of heat transfer is maximum. It is mainly due to higher rates of unsteadiness downstream of the cylinder. Rotating the cylinder up to RS=2 decreases the vortex shedding mechanism and consequently decreases the rate of heat transfer between the rotating cylinder and the fluid flow. Beyond the RS=2, due to development of a significant rotating flow over the cylinder, the rate of heat transfer does not change, significantly. As a result, both of the vortex shedding mechanism and the rotational effect have an influence on the rate of heat transfer.

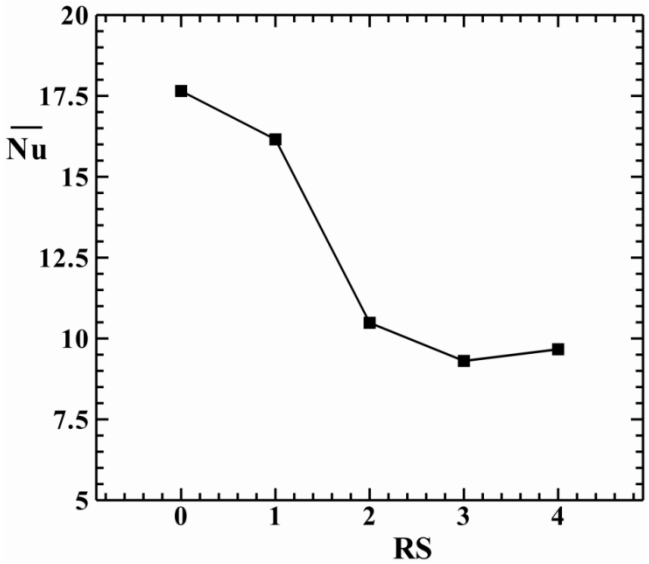

Figure13. *Variation of time-averaged mean Nusselt number with rotating speed*

6. CONCLUSION

Convective heat transfer and fluid flow over a rotating cylinder at Re=200 under different rotating speeds in the range of $0 \leq RS \leq 4$ were numerically investigated in the present study for constant Prandtl number of 7.0. It was found that rotating the cylinder reduces the instabilities of the shear layer by suppressing the wake downstream of the cylinder. In this situation, the oscillation amplitudes of the exerted forces on the cylinder attenuate proportional to the RS. However, due to an increase in the pressure difference on the half-upper and half-lower sides of the rotating cylinder, the magnitude of the lift coefficient enhances while the value of the drag coefficient reduces compared with those of the stationary cylinder. Furthermore, rotating the cylinder attenuates the vortex shedding mechanism at small rotating speeds and eliminates the shedding effects at high rotating speeds by suppressing the wake downstream of the cylinder. On the other hand, it was demonstrated that both instabilities of the shear layer and rotational effect are important on the heat exchange rate between the fluid flow and hot cylinder. In general, rotating the cylinder reduces the value of the mean Nusselt number compared with that of the stationary cylinder. However, at high RS values, due to development of the uniform rotating flow over the cylinder, the rate of local heat transfer becomes same for each individual location on the cylinder.

REFERENCES

[1] S. Kang, Uniform-shear flow over a circular cylinder at low Reynolds numbers, J. Fluids Struct. 22 (2006) 541–555.

[2] B.N. Rajani, A. Kandasamy, S. Majumdar, Numerical simulation of laminar flow past a circular cylinder, Appl. Math. Model. 33 (2009) 1228–1247.

[3] H.L. Zhang, N.W.M. Ko, Numerical analysis of incompressible flow over smooth and grooved circular cylinders, Comput. Fluids. 25 (3) (1996) 263-281.

[4] L. Perret, PIV investigation of the shear layer vortices in the near wake of a circular cylinder, Exp. Fluids. 47 (2009)789–800.

[5] C.H.K Williamson, Vortex dynamics in the cylinder wake, Annu. Rev. Fluid. Mech. 28 (1996) 477-539.

[6] Y. Yokoi, K. Kamemoto, Vortex Shedding from an Oscillating Circular Cylinder in a Uniform Flow,Exp. Therm. Fluid Sci. 8 (1994) 121-127.

[7] A. Rao, M.C. Thompson, T. Leweke, K. Hourigan, Flow past a rotating cylinder translating at different gap heights along a wall, J. Fluids Struct. 57 (2015) 314–330.

[8] Rao, B.E. Stewart, M.C. Thompson, T. Leweke, K. Hourigan, Flows past rotating cylinders next to a wall, J. Fluids Struct. 27 (2011) 668–679.

[9] Dipankar, T.K. Sengupta, Flow past a circular cylinder in the vicinity of a plane wall, J. Fluids Struct. 20 (2005) 403–423.

[10] M. Abrahamsen Prsic, M. Chen Ong, B. Pettersen, D. Myrhaug, Large Eddy Simulations of flow around a circular cylinder close to a flat seabed, Mar. struct. 46 (2016) 127-148.

[11] F. Afroz, M. A. R. Sharif, A. Lang, Numerical study of adverse pressure gradient generation over a flat plate using a rotating cylinder, J. Fluids Struct. 62 (2016) 187–208.

[12] P. Thakur, S. Mittal, N. Tiwari, R. P. Chhabra, The motion of a rotating circular cylinder in a stream of Bingham plastic fluid, J. Nonnewton. Fluid Mech. 235 (2016) 29–46.

[13] S.J. Karabelas, Large Eddy Simulation of high-Reynolds number flow past a rotating cylinder, Int. J. Heat Fluid Flow.31 (2010) 518–527.

[14] K.M. Lam, Vortex shedding flow behind a slowly rotating circular cylinder, J. Fluids Struct. 25 (2009) 245–262.

[15] J. Ghazanfarian, M.R.H. Nobari, A numerical study of convective heat transfer from a rotating cylinder with cross-flow oscillation, Int. J. Heat Mass Transf. 52 (2009) 5402–5411.

[16] U. Ikhtiar, S. Manzoor, N.A. Sheikh, M. Ali, Free stream flow and forced convection heat transfer around a rotating circular cylinder subjected to a single gust impulse, Int. J. Heat Mass Transfer. 99 (2016) 851–861.

[17] D. Chatterjee, C. Sinha, Effect of Prandtl number and rotation on vortex shedding behind a circular cylinder subjected to cross buoyancy at subcritical Reynolds number, Int. Commun. Heat Mass Transf. 70 (2016) 1–8.

[18] S.B. Paramane,A. Sharma, Heat and fluid flow across a rotating cylinder dissipating uniform heat flux in 2D laminar flow regime, Int. J. Heat Mass Transf. 53 (2010) 4672–4683.

[19] R. Hassanzadeh, Effects of Unsteady Flow Generation Over a Hot Plate on the Cooling Mechanism Using a Rotating Cylinder, Arab. J. Sci. Eng. (2017) Doi: 10.1007/s13369-017-2911-6.

[20] M. Darvishyadegari, R. Hassanzadeh, Convective heat transfer and fluid flow of two counter-rotating cylinders in tandem arrangement, Acta Mech. (2017) doi: 10.1007/s00707-017-2070-6.

[21] S.V. Patankar, Numerical Heat transfer and Fluid Flow, Taylor & Francis, New York, 1980.

[22] Q.M. Al-Mdallal, Numerical simulation of viscous flow past a circular cylinder subject to a circular motion, Eur. J. Mech. B. Fluids. 49 (2015) 121–136.

[23] R.D. Henderson, Nonlinear dynamics and patterns in turbulent wake transition, J. Fluid Mech. 352 (1997) 65–112.

[24] J.R. Meneghini, P.W. Bearman, Numerical simulation of high amplitude oscillatory flow about a circular cylinder, J. Fluids Struct. 9 (1995) 435–455.

[25] C.Y. Wen, C.Y. Lin, Two-dimensional vortex shedding of a circular cylinder, Phys. Fluids. 13 (2001) 557–560.

[26] P. Poncet, Topological aspects of three-dimensional wakes behind rotary oscillating cylinders, J. Fluid Mech. 517 (2004) 27–53.

[27] N. Mahir, Z. Altaç, Numerical investigation of convective heat transfer in unsteady flow past two cylinders in tandem arrangements, Int. J. Heat Fluid Flow. 29 (2008) 1309–1318.

[28] Liu, X. Zheng, C.H. Sung, Preconditioned multigrid methods for unsteady incompressible flows, J. Comput. Phys. 139 (1998) 35–37.

[29] H. Ding, C. Shu, Y.O. Yeo, D. Xu, Numerical simulation of flows around two circular cylinders by mesh-free least square-based finite difference methods, Int. J. Numer. Meth. Fluids. 53(2007) 305–332.

[30] M. Braza, P. Chassaing, H. Ha Minh, Numerical study and physical analysis of the pressure and velocity fields in the near wake of a circular cylinder, J. Fluid Mech. 165(1986) 79–130.

[31] Hilpert, R., Forsch, Geb., 1933. Ingenieurwes 4, 215.

[32] S.W. Churchill, M. Bernstein, A Correlation Equation for Forced Convection from Gases and Liquids to a Circular Cylinder in Cross Flow, J. Heat Transfer, Trans. ASME. 94 (1977) 300-306.

[33] Harimi, M. Saghafian, Numerical simulation of fluid flow and forced convection heat transfer from tandem circular cylinders using overset grid method, J. Fluids Struct. 28 (2012) 309–327.

Citation: *Rahim Hassanzadeh, Mohsen Darvishyadegari, (2018)" Influence of Rotation on the Heat and Fluid Flow around a Circular Cylinder",* ***International Journal of Modern Studies in Mechanical Engineering, 4(4), pp. 16-29. DOI: http://dx.doi. org/10.20431/2454-9711.0404003***